J|A|C|S
ARTICLES
Published on Web 11/16/2005

Observing Capillarity in Hydrophobic Silica Nanotubes

Karthik Jayaraman, Kenji Okamoto,§ Sang Jun Son, Charles Luckett, Azeem H. Gopalani, Sang Bok Lee,* and Douglas S. English*

Contribution from the Department of Chemistry and Biochemistry, University of Maryland, College Park, Maryland 20742

Received August 12, 2005; E-mail: slee@umd.edu; denglish@umd.edu

Abstract: The development of template-synthesized silica nanotubes has created a unique opportunity for studying confined fluids by providing nanometer-scale containers in which the inner diameter (i.d.) and surface chemistry can be systematically and independently varied. An interesting question to be answered is the following: do solvents wet nanometer-scale tubes in the same way they wet ordinary capillaries? To answer this question, we have conducted studies to explore the wettability of the hydrophobic interiors of individual nanotubes. In these studies, single nanotubes with i.d.'s of either 30 or 170 nm were investigated over a range of water/methanol mixtures. These studies provide a direct route for comparing wetting phenomena in nanotubes with conventional macroscopic theories of capillarity. Our observations reveal four important aspects of capillary wetting in the 30−170 nm regime, a size range where the application of the Young−Laplace theory has not been experimentally investigated for hydrophobic pores. They are (i) a sharp transition between wetting and nonwetting conditions induced by addition of a cosolvent, (ii) invariance of this transition between nanotubes of 30 and 170 nm pore diameter, (iii) failure of the Young−Laplace equation to accurately predict the cosolvent's (methanol) mol fraction where the transition occurs, and (iv) reversibility of the observed wetting. The first two aspects conform to conventional capillarity (Young−Laplace), but the latter two do not. These measurements were complemented with ensemble experiments. The difference between theory and experiment is likely due to reliance on macroscopic values of contact angles or to liquid-phase instability within the hydrophobic pore.

Introduction

The template-guided synthesis of nanotubes was pioneered by Martin and co-workers.[1,2] Their methods can be used to produce nanotubes from a variety of materials over a wide range of size scales. Nanotubes produced from this method promise to have a broad range of important applications. For instance, nanotubes produced from metals[3−5] have been used in chemical separations and those made of conducting polymers show promise for use in fast-response electrochromic displays.[6] Membranes composed of silica nanotubes are readily formed from template-based sol−gel synthesis and have been used for bioseparations.[2,7,8] Free-standing nanotubes have been used for the capture, transport, and delivery of target molecules.[2,5,9] Of particular interest is the use of nanotubes for the delivery or uptake of biomolecules and drugs. For example, Son et al. have recently reported the synthesis of magnetic nanotubes and their use for magnetic field assisted separations, biointeractions, and drug delivery.[10]

A barrier to overcome in applications of nanotubes as vehicles for biomolecules will be the ability to fill, transport and release molecules in a controlled manner. An elegant solution for controlled release of nanotube contents was recently proposed and involves the use of nano "test tubes" where one end is open and the other is permanently sealed. The open end could be reversibly capped to hold the contents until release is triggered.[11] In principle, this approach offers the possibility for controlled release of cargo molecules. However, the filling of nano test tubes will be far from trivial, and fundamental questions remain pertaining to the transport of molecules into, out of, or even near nanostructured materials. A relevant example was demonstrated by Mei and co-workers in which dye molecules were shown to avoid entering spheroidal cavities formed in poly(vinyl alcohol) films immersed in methanol.[12,13] The source of this unusual behavior is possibly due to unexpected wetting

§ Present address: Department of Chemistry, Graduate School of Science, Kyoto University, Japan.

(1) (a) Martin, C. R. *Science* **1994**, *266*, 1961. (b) Lakshmi, B. B.; Patrissi, C. J.; Martin, C. R. *Chem. Mater.* **1997**, *9*, 2544.
(2) Martin, C. R.; Kohli, P. *Nat. Rev. Drug Discovery* **2003**, *2*, 29.
(3) Wirtz, M.; Parker, M.; Kobayashi, Y.; Martin, C. R. *Chem. Eur. J.* **2002**, *8*, 3573.
(4) Lee, S. B.; Martin, C. R. *J. Am. Chem. Soc.* **2002**, *124*, 11850.
(5) Kohli, P.; Martin, C. R. *Drug News Perspect.* **2003**, *16*, 566.
(6) Cho, S. I.; Kwon, W. J.; Choi, S. J.; Kim, P.; Park, S. A.; Kim, J.; Son, S. J.; Xiao, R.; Kim, S. H.; Lee, S. B. *Adv. Mater.* **2005**, *17*, 171.
(7) Lee, S. B.; Mitchell, D. T.; Trofin, L.; Nevanen, T. K.; Soderlund, H.; Martin, C. R. *Science* **2002**, *296*, 2198.
(8) Mitchell, D. T.; Lee, S. B.; Trofin, L.; Li, N. C.; Nevanen, T. K.; Soderlund, H.; Martin, C. R. *J. Am. Chem. Soc.* **2002**, *124*, 11864.
(9) Hou, S. F.; Harrell, C. C.; Trofin, L.; Kohli, P.; Martin, C. R. *J. Am. Chem. Soc.* **2004**, *126*, 5674.
(10) Son, S. J.; Reichel, J.; He, B.; Schuchman, M.; Lee, S. B. *J. Am. Chem. Soc.* **2005**, *127*, 7316.
(11) Gasparac, R.; Kohli, P.; Mota, M. O.; Trofin, L.; Martin, C. R. *Nano Lett.* **2004**, *4*, 513.
(12) Mei, E.; Sharonov, A.; Ferris, J. H.; Hochstrasser, R. M. *Appl. Phys. Lett.* **2005**, *86*, 043102.
(13) Mei, E.; Sharonov, A.; Gao, F.; Ferris, J. H.; Hochstrasser, R. M. *J. Phys. Chem. A* **2004**, *108*, 7339.

10.1021/ja055535c CCC: $30.25

patterns on the nanopatterned surfaces.[13] Likewise, wetting processes will play a critical role in the transport of solute molecules in and out of nanotubes. Our methods allow direct measurements of wetting in individual nanotubes or in nanotube membranes and provide a way to compare wetting on patterned surfaces with individual features and directly test theories of wetting and capillarity. These are the goals of this article.

It has long been understood that wetting of a solid surface is determined by the relative sizes of the free energy changes per unit area (γ) associated with the formation of the liquid/vapor, solid/liquid, and solid/vapor interfaces. Mathematical treatment of these competing forces at the vapor/liquid/solid interface gave rise to the Young equation in 1805.[14] In the same year the Young−Laplace equation was introduced to describe capillarity:[14]

$$\Delta P = \frac{2\gamma \cos \theta_c}{r} \quad (1)$$

where ΔP is the capillary pressure, γ is the surface tension of liquid,[15] θ_c is the contact angle of the liquid with the capillary wall, and r is the capillary radius. The Young and Young−Laplace equations accurately describe the wetting of plane surfaces by liquid drops and the rise or depression of liquids in glass capillaries as well as a host of other processes. In nanoscale enclosures, phenomena such as capillary condensation, dry layers, and spontaneous drying can lead to observations that are not predicted by these classic equations.[16] Hence, the behavior of water in hydrophobic confinement presents interesting theoretical and experimental challenges.[17] Recent theoretical predictions suggest that water bounded by closely spaced extended hydrophobic surfaces may be inherently unstable.[18−21] This instability occurs when the chemical potentials of the liquid and vapor are comparable. Calculations based on the Kelvin equation show that liquid water may be unstable, relative to its vapor phase, when confined between two hydrophobic surfaces separated by distances on the order of 10^2 nm.[19] Giaya and Thompson have conducted simulations of liquid-phase stability in nanoscale cylindrical pores of varying size (0.1−1000 nm) and over a range of solvent/surface interaction potentials.[21] They plotted the observed phase behavior as a function of these two variables. Their results conclude that in the case of a noninteracting wall and solvent, liquid/vapor coexistence can occur in cylindrical pores with diameters of several micrometers. These predictions suggest that models for capillarity in nanotubes may need to be revised to encompass these possibilities. In this context, experimental results are needed to help test emerging theories of capillarity, particularly in hydrophobic cases. Our earlier work demonstrated the feasibility of using individual nanotubes to provide experimental results for wetting, diffusion, and phase stability in nanometer cylindrical pores.[22] In this paper we describe additional single-nanotube studies aimed at providing experimental insight for developing theoretical descriptions of capillary wetting in nanoscale containers and compare their results with those from nanotube membranes.

Table 1. Contact Angles of Methanol/Water Mixtures on an OTS Surface and the Predicted Capillary Pressure for 30 and 170 nm Nanotubes

X_{MeOH}	θ_c (deg)[a]	ΔP_{170nm} (atm)	ΔP_{30nm} (atm)[b]
0.0	102	−3.5	−20
0.05	92	−0.4	−2.4
0.13	76	2.6	15
0.31	65	3.2	18
0.57	34	5.4	31
1.0	10	5.9	28

[a] Advancing contact angles (θ_c) were measured for each solvent on an OTS-coated glass coverslip. [b] Pressure differences were calculated using eq 1.

We have conducted measurements of solvent wetting, solute diffusion, and surface dielectric properties in both 30 and 170 nm inner diameter (i.d.) nanotubes as a function of methanol concentration in binary mixtures with water. Surface sol−gel (SSG) template synthesis[23,24] was used to obtain silica nanotubes of different diameters, and the interior surfaces were made hydrophobic by the covalent attachment of octadecyltrimethoxysilane (OTS).[5,7,8] OTS renders silica surfaces hydrophobic as shown by measurements of advancing contact angles on planar silica substrates (Table 1). The use of hydrophobically modified nanotubes (henceforth referred to as hydrophobic nanotubes) was chosen for its relevance to theoretical studies of the hydrophobic effect in confined environments and to complement our previous work.[22] Our studies provide much needed experimental results covering a range of solvent concentrations and nanotube sizes that are relevant to modern theoretical approaches to understanding nanoscale wetting and capillarity.[17−19,21]

Experimental Section

Materials. Hexanes, concentrated sulfuric acid, and hydrogen peroxide (30%) were purchased from Fisher Scientific. Methanol, glacial acetic acid, and concentrated hydrochloric acid were purchased from J. T. Baker. Silicon(IV) tetrachloride was purchased from ACROS Organics. Octadecyltrimethoxysilane (OTS, 95% purity) was purchased from Gelest Inc., and tetraethoxysilane (TEOS, 99.999% purity) was purchased from Aldrich. For the production of 170 nm i.d. nanotubes, commercial alumina membranes (Anodisc 47, catalog no. 6809-5022) with 0.2 μm pore size were purchased from Whatman. Alumina membranes with 60 nm pores, for the production of 30 nm i.d. nanotubes, were produced in-house. Nile red and 1,1′-dioctadecyl-3,3,3′,3′-tetramethylindocarbocyanine perchlorate ($DiIC_{18}$) were purchased from Molecular Probes. Ethanol (95%) was purchased from AAPER Alcohol. All solvents were reagent grade, with the exception of HPLC grade methanol and hexanes, and all were used without further purification.

Synthesis of Silica Nanotube Membranes and Silica Nanotubes. Silica nanotubes with 170 and 30 nm i.d.'s and lengths of 10−15 μm were synthesized using layer-by-layer template synthesis. Commercially available alumina templates were used to synthesize 170 nm tubes, and templates for synthesizing 30 nm tubes were fabricated in-house using the procedure detailed elsewhere.[25] The SSG procedure detailed

(14) Adamson, A. W.; Gast, A. P. *Physical Chemistry of Surfaces*; John Wiley & Sons: New York, 1997.
(15) Young, T. F.; Harkins, W. D. *International Critical Tables of Numerical Data*; McGraw-Hill: New York, 1926.
(16) Helmy, R.; Kazakevich, Y.; Ni, C.; Fadeev, A. Y. *J. Am. Chem. Soc.* **2005**, *127*, 12446.
(17) Ball, P. *Nature (London)* **2003**, *423*, 25.
(18) Luzar, A. *J. Phys. Chem. B* **2004**, *108*, 19859.
(19) Lum, K.; Chandler, D.; Weeks, J. D. *J. Phys. Chem. B* **1999**, *103*, 4570.
(20) (a) ten Wolde, P. R.; Sun, S. X.; Chandler, D. *Phys. Rev. E* **2002**, *65*, 011201. (b) Maibaum, L.; Chandler, D. *J. Phys. Chem. B* **2003**, *107*, 1189.
(21) Giaya, A.; Thompson, R. W. *J. Chem. Phys.* **2002**, *117*, 3464.
(22) Okamoto, K.; Shook, C. J.; Bivona, L.; Lee, S. B.; English, D. S. *Nano Lett.* **2004**, *4*, 233.
(23) Kohli, P.; Martin, C. R. *Curr. Pharm. Biotechnol.* **2005**, *6*, 35.
(24) Kovtyukhova, N. I.; Mallouk, T. E.; Mayer, T. S. *Adv. Mater.* **2003**, *15*, 780.
(25) (a) Masuda, H.; Fukuda, K. *Science* **1995**, *268*, 1466. (b) Li, A. P.; Muller, F.; Birner, A.; Nielsch, K.; Gosele, U. *J. Appl. Phys.* **1998**, *84*, 6023.

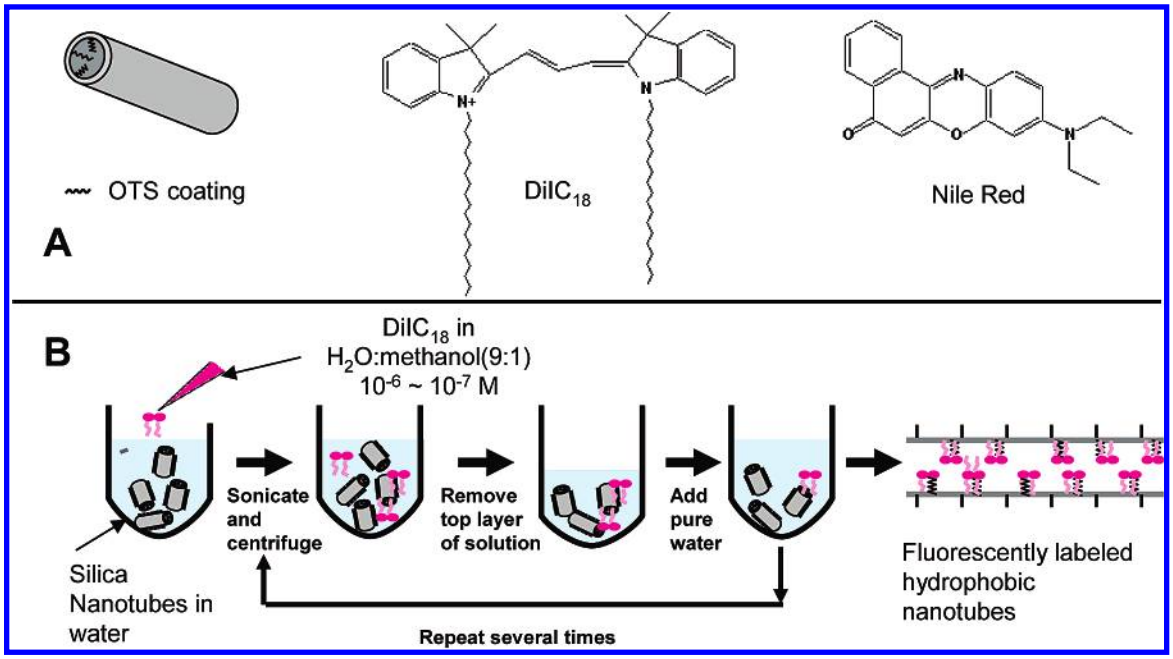

Figure 1. Introduction of dye to the OTS-modified hydrophobic nanotube interiors. (A) OTS-modified silica nanotubes were stained with either $DiIC_{18}$ or nile red by physisorption to the hydrophobic interior surface. The surfactant-like fluorescent dye, $DiIC_{18}$, was used in FRAP experiments, and the solvatochromic dye, nile red, was used as a reporter of local dielectric properties inside individual nanotubes. Both dyes partition well to the hydrophobic interface and only trace amounts were used to ensure that the nanotube's internal surface properties were not significantly altered by the adsorbed dyes. (B) Step-by-step scheme showing the procedure for the introduction of $DiIC_{18}$ to the nanotube interior. Nile red was introduced in an analogous manner.

previously[2,23,24] was used to obtain silica nanotube membranes. Wall thicknesses of 2−15 nm can be obtained by varying the deposition cycles in the SSG synthesis. Nanotubes with hydrophobic interior surface were produced by immersing the silica-coated surfaces in a solution of 5% (v/v) octadecyltrimethoxysilane and 16 mM acetic acid in ethanol/water (95% v/v) for 30 min at room temperature followed by rinsing with ethanol and curing at 150 °C for 2 h. The intact silica nanotube membrane with hydrophobic interior surface was used for the membrane transport and membrane resistance (ac impedance) measurements. To obtain free-standing nanotubes from the membrane, both faces of the sol−gel-treated template membrane were mechanically polished to remove the silica surface layers and expose the underlying template alumina. The template was then dissolved by immersing the membranes overnight in a 25% (w/w) aqueous solution of H_3PO_4. The liberated nanotubes are then filtered from the acid solution and repeatedly rinsed with deionized water.

Fluorophore Adsorption. Dye was introduced to the nanotube interior by immersion of nanotubes in a $DiIC_{18}$ or nile red solution (10^{-7} M) of water/methanol (9:1 v/v). Sonication is used to disperse the nanotubes and to facilitate filling of the nanotube with the dye solution. Filling of the nanotubes did not occur without sonication. After sonication, the sample is centrifuged to concentrate the nanotubes. The supernatant is removed and nanotubes are suspended in deionized water. The sonication−centrifuge−rinse steps are repeated several times, after which the solution is diluted with deionized water and stored in the dark until needed. Figure 1 shows the schematic of the procedure for introducing dye to the nanotube interior. $DiIC_{18}$ has two hydrophobic tails and a charged indocarbocyanine headgroup and partitions well to the OTS interface in polar solvents. Nile red, which has been used as a sensitive probe of microenvironements in sol−gel films,[26] is also sequestered in the hydrophobic nanotube interior when introduced using the procedure described above. Care was taken to use only trace amounts of these dyes, corresponding to an average of 1 dye molecule per 20 nm^2, at concentrations which do not significantly alter the contact angle of the immersing solvent with the substrate.[22]

(26) Martin-Brown, S. A.; Fu, Y.; Saroja, G.; Collinson, M. M.; Higgins, D. A. *Anal. Chem.* **2005**, *77*, 486.

Sample Preparation and Imaging of Immobilized Nanotubes. Immobilization, confocal imaging, and FRAP experiments were described previously.[22] FRAP measurements were used to measure diffusion coefficients of the entrapped molecules inside nanotubes of 170 and 30 nm i.d. in a range of water−methanol mixtures. FRAP experiments were conducted over a period of 2 consecutive days to ensure that equilibrium had been reached for each sample. Under strongly wetting conditions ($X_{MeOH} > 0.5$ in the case of both nanotube diameters) rapid modulation of the laser beam was necessary for accurate observation of recovery. In these experiments an acousto-optic modulator (model C8217A, NEC USA, New York) driven by a model DE, VCO deflector driver (Intraaction, Bellwood, IL) was used to rapidly adjust the beam intensity. The detector, an avalanche photodiode (APD), was gated to avoid overexposure during photobleaching (high laser intensity). LabView (National Instruments, Austin, TX) was used to synchronize the APD gating and laser intensity. An example of data acquired in this way is shown in Figure 3E. In this paper we have also employed the use of spectroscopic imaging in which emission spectra are acquired from individual locations on a single nanotube. Spatially resolved fluorescence spectra were collected from individual points in the fluorescence image by positioning the focal point (370 nm fwhm) of the excitation laser at the desired image locations by using a piezo-actuated positioning stage with closed loop feedback (Nanobio II, Mad City Lab, Madison, WI). A polychromator (Acton Research Corp., Acton, MA) equipped with a charge-coupled device (CCD, Roper Scientific, Trenton, NJ) was used to collect and record emission spectra from the microscope image point.

Transport Experiments. Bulk transport experiments with 170 nm hydrophobic nanotube membranes were conducted using a simple U-tube setup described previously.[4] Briefly, the nanotube membrane was mounted between the two halves of the U-tube permeation cell. Feed solution was 5 mL of 4.6×10^{-5} M $DiIC_{18}$ in the solvent under investigation. Receiver solution was 5 mL of same solvent without $DiIC_{18}$. Both feed and receiver solutions were stirred during permeation experiments, and transport occurred across the membrane by diffusion of permeate down the concentration gradient. Transport from feed solution to the permeate solution was monitored by UV−vis absorbance

Table 2. Molar Extinction Coefficients and Maximum Absorption Wavelength Values ($\lambda_{max,abs}$) for $DiIC_{18}$ at Various Mole Fractions of Methanol in Water

X_{MeOH}	ϵ (M^{-1} cm^{-1})	$\lambda_{max,abs}$ (nm)
0.05	45 000	561
0.13	47 000	561
0.31	62 000	549
0.57	98 000	549
1.0	186 000	549

of $DiIC_{18}$ using the molar extinction coefficients and wavelengths given in Table 2. Experiments were stopped once 5% of the permeate ion was transported across the membrane from feed to receiver solution.

Membrane Resistance Measurements (ac Impedance). The same U-tube setup used in the membrane transport experiment was used for the ac impedance measurement to find the membrane resistance. Both half-cells in the U-tube setup were filled with 25 mL of 0.1 M KCl aqueous solution with 0, 0.05, 0.13, 0.31, and 0.57 mol fractions of methanol. A Ag/AgCl electrode was immersed into each cell as working and reference electrodes, and a Pt counter electrode was used in one half-cell. Impedance data were obtained and analyzed with a model 660A potentiostat (CH instrument, Austin, TX) using a ±20 mV sinusoidal potential applied across the membrane over a frequency range of $0.1-10^5$ Hz.

Results

Figure 2A shows the uniform nanotube size distribution (i.d. = 30 nm) obtained using an improved layer-by-layer SSG template synthesis method.[9,24] These nanotubes were synthesized from a template membrane with a pore diameter of 60 nm and thickness of 12 μm. To achieve a wall thickness of 15 nm, nine layers were sequentially deposited in the SSG process.[24] TEM and confocal fluorescence imaging confirm that the layer-by-layer SSG method provides a higher degree of surface uniformity than our previous method where the wall thickness depended on immersion time and sol concentration.[22] The marked improvement in surface homogeneity is seen in the confocal fluorescence image in Figure 2B showing a hydrophobic nanotube containing trace amounts of the fluorophore $DiIC_{18}$. Previously we observed irregularities such as dim or bright regions in fluorescence images of nanotubes which were assigned to inner surface bulges or constrictions.[22,27] Such irregularities are nearly absent with the new synthesis method. A surprising difference in nanotube lengths was noted when comparing TEM and fluorescence images. In Figure 2A, long nanotubes are visible in the TEM image, but such long tubes are never observed in our fluorescence images suggesting that breakage occurs during the sample preparation processes. These processes include introduction of dye to the nanotube interior (Figure 1B) and immobilization of nanotubes on a glass coverslip. During these steps nanotubes are apparently fragmented into shorter pieces. The average length of the nanotubes included in this study was 7 μm.

FRAP Studies. FRAP experiments were used to monitor the diffusion of adsorbed probe molecules inside an immersed nanotube. A FRAP experiment is conducted by imaging a nanotube in the confocal microscope and then positioning the focused laser beam on a region of the nanotube for 10−20 s.

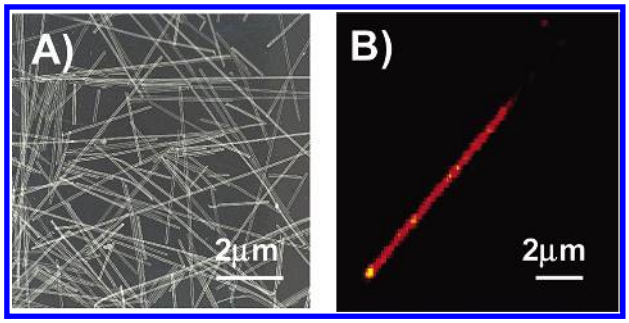

Figure 2. Microscope images of differentially modified silica nanotubes. (A) A TEM image of nanotubes with 30 nm i.d. and internally modified with OTS. (B) Laser-scanning confocal fluorescence image of a single 30 nm i.d. nanotube. The interior surface contains a trace amount of the fluorescent dye, $DiIC_{18}$. Prior to imaging, the nanotube was immobilized on a glass coverslip under water.

The laser intensity is adjusted so that dye molecules in the illuminated spot will undergo rapid and irreversible photochemistry leaving them non emissive, i.e., photobleached. The recovery of the fluorescence signal occurs when unbleached fluorophores diffuse into the bleached region and is a convenient way to measure diffusion of the fluorophore.

Figure 3 illustrates the two limiting cases that were observed in FRAP experiments with dye-bearing nanotubes. Panels A and B in Figure 3 are images of a hydrophobic nanotube in *pure water* before and after photobleaching. The four green arrows denote locations where an intense bleaching beam was focused to induce irreversible photobleaching of the local dye molecules. Figure 3A shows the nanotube prior to bleaching. Figure 3B shows the same nanotube imaged 26 min after bleaching was completed. In pure water the bleached regions persist indefinitely, indicating that there is *no measurable diffusion of the dye molecules*. Panels C and D in Figure 3 reveal a starkly different behavior when the nanotubes are immersed in *pure methanol*. Here, the *entire nanotube* shows a greatly diminished intensity caused by photobleaching of dye at a single well-defined spot. This effect is due to the *rapid diffusion of the dye molecules* during and after photobleaching. The rapid exchange of dyes within the laser spot during the bleaching period and diffusion of bleached dye throughout the nanotube results in decreased emission intensity over the entire nanotube. The very different observations from the two solvents are due to their respective wetting strengths at the nanotube interior. In pure water, the absence of diffusion indicates that the nanotube interior is dry. This assignment is supported by observations from single-molecule fluorescence correlation spectroscopy studies which show that $DiIC_{18}$ can diffuse freely at the interface between water and a dimethyloctadecylsiloxane surface.[28] Therefore, FRAP should be observed if a water−OTS interface does exists inside of a nanotube. Furthermore, on the basis of predictions and observations of capillarity at the macroscale one should expect that the hydrophobic nanotube interior is dry in water and filled in methanol. For instance, an OTS-coated capillary of 0.5 mm i.d. shows a capillary depression of 0.79 cm in pure water and a rise of 0.88 cm in pure methanol. When the nanotube is filled in methanol it was necessary to conduct FRAP experiments with a higher temporal resolution than is achievable by acquiring sequential confocal images. Accordingly, experiments were conducted using an acousto-optic

(27) Okamoto, K.; Jayaraman, K.; Son, S. J.; Lee, S. B.; English, D. S. In *Dekker Encyclopedia of Nanoscience and Nanotechnology*; Schwarz, J. A., Contescu, C. I., Putyera, K., Eds.; Taylor and Francis Group: New York, 2004.

(28) Wirth, M. J.; Swinton, D. J. *Anal. Chem.* **1998**, *70*, 5264.

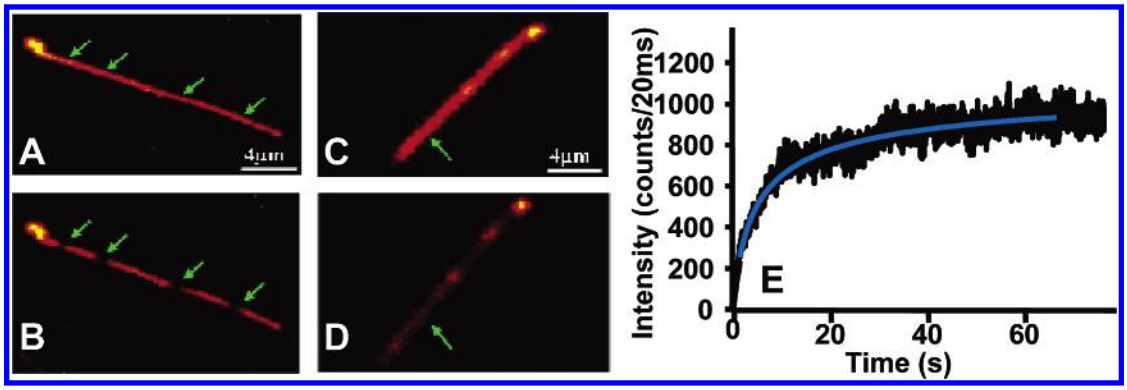

Figure 3. Examples of FRAP experiments conducted with 30 nm i.d. nantoubes under nonwetting conditions in water and strongly wetting conditions in methanol. (A) Confocal fluorescence image of a $DiIC_{18}$-bearing hydrophobic nanotube immersed in water just prior to conducting the FRAP experiment. The green arrows indicate four spots which were arbitrarily chosen for photobleaching. (B) A confocal image obtained 26 min after photobleaching was conducted showing that under pure water no FRAP is observed. The lack of diffusion-induced recovery suggests that the nanotube interior remains dry when immersed in water as expected for a hydrophobic capillary. (C and D) Confocal images of a hydrophobic nanotube before and after conducting a FRAP experiment in methanol. Here, bleaching was conducted at a single spot shown by the green arrow. In contrast to the experiment conducted in water, a decrease in emission was observed over the entire nanotube interior. The wide-spread bleaching occurs because of rapid diffusion by $DiIC_{18}$ in the nanotube interior. As molecules are bleached, they rapidly diffuse away diluting the concentration of fluorophores over the entire nanotube. Facile diffusion in the nanotube indicates that hydrophobic nanotube interior has been filled by methanol. (E) Fluorescence recovery curve demonstrating the rapid recovery observed in pure methanol. This data was used to calculate the diffusion coefficient for $DiIC_{18}$ in the methanol-filled nanotube by using eqs 2 and 3. The calculated value is 8.7×10^{-7} cm^2/s.

modulator to switch the laser intensity, as described in the Experimental Section. This method provides enough time resolution to achieve an accurate measurement of the fluorescence recovery as shown in Figure 3E. The fluorescence intensity, *I(t)*, in Figure 3E was fit to the following equation:[29]

$$I(t) = I(\infty) - G(t) \tag{2}$$

where $I(\infty)$ is the intensity after recovery is complete. $G(t)$ is given eq 3:

$$G(t) = \frac{B}{\left(1 + 4\frac{Dt}{s^2}\right)^{1/2}} \tag{3}$$

where B is the bleach depth, s^2 is the beam spot variance, and D is the diffusion coefficient of the fluorophore. The diffusion coefficient calculated for the data in Figure 3E is about one-third of the value obtained for $DiIC_{18}$ on planar C_{18}/water interfaces obtained by single-molecule fluorescence correlation spectroscopy.[28,30] It is interesting that the dye remains within the nanotube even in pure methanol, a good solvent for this dye. The lower diffusion coefficient may reflect stronger adsorption at the curved interface relative to that of the planar C_{18}/water interface, and this could explain why the dye remains in the nanotube.

Spectroscopic Imaging. We used the solvatochromism of nile red to gauge the local dielectric properties of the OTS-modified nanotube interior surface. Figure 4A contains spectra acquired from nile red in four different solvents ranging from heptane to a mixture of 2% (v/v) methanol in water. As the polarity of the solvent increases, the wavelength of maximum emission (λ_{max}) increases. This solvatochromic property is used to provide further confirmation that our nanotube interiors are in fact dry in water and wetted in methanol. Figure 4B shows the emission spectra for nile red acquired from the same single nanotube immersed first in water and then in methanol. Prior

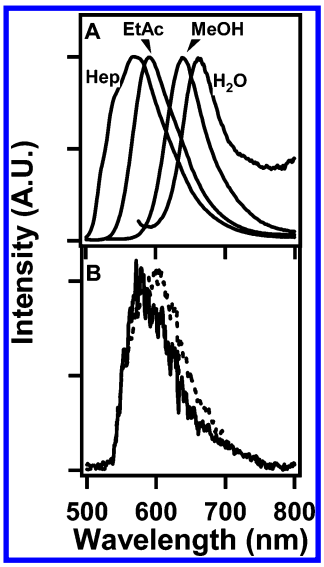

Figure 4. Nile red fluorescence spectra acquired in different solvents and from a single silica nanotube. (A) Nile red emission in heptane, ethyl acetate, methanol, and water. In water, a small proportion (2%) of methanol was added to aid dissolution. (B) Emission spectra from nile red inside an OTS-modified nanotube. The nanotube was initially immersed under water (—) and then under methanol (- - -). The spectrum acquired from the dry nanotube prior to the addition of water (data not shown) overlays well with the spectrum in water, λ_{max}.

to immersion the emission from this nanotube was collected in air (data not shown) and had a λ_{max} of 580 nm. The sample cell was then filled with water, and the λ_{max} from the same nanotube was observed to remain unchanged. The values in air and water correspond well to the value measured for nile red dissolved in the moderately nonpolar solvent ethyl acetate. This similarity suggests that an effective dielectric, determined by the proximities of the OTS alkyl chains, the polar nanotube surface, and the siloxane anchor, is reported by nile red at the nanotube interior surface. The sample cell was next filled with methanol and the nile red λ_{max} value changed to 605 nm. The observed red shift in λ_{max} indicates that the polarity of the probe environment increased as the nanotube interior filled with

(29) Thompson, N. L.; Burghardt, T. P.; Axelrod, D. *Biophys. J.* **1981**, *33*, 435.
(30) Korlach, J.; Schwille, P.; Webb, W. W.; Feigenson, G. W. *Proc. Natl. Acad. Sci. U.S.A.* **1999**, *96*, 8461.

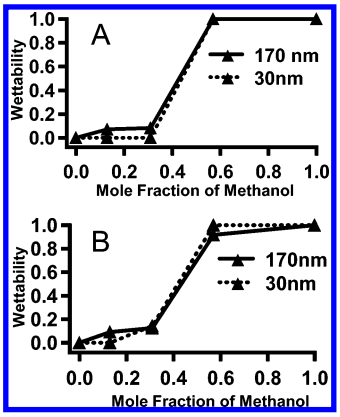

Figure 5. Solvent-dependent wettability of 30 and 170 nm nanotubes. (A) Wettability of the hydrophobic nanotube interior over a range of methanol mol fractions for both 30 and 170 nm nanotube internal diameters. The transition from nonwetting to wetting conditions occurs between 0.31 and 0.57 methanol mol fraction for both nanotube sizes. (B) Wettability of both nanotube sizes after equilibration for 24 h.

methanol. As seen in Figure 4A, nile red has a λ_{max} of 638 nm in pure methanol. The lower value of λ_{max} measured in the nanotube simply indicates that the probe environment is still impacted by the C_{18} interface. It is impossible to determine where the nile red is located relative to the surface; however, it may be possible to selectively excite subpopulations of nile red to distinguish between emission from molecules at the C_{18} layer and from those solvated in methanol, and this will be attempted in future work. Additionally, we are currently developing the use of a covalently linked nile red analogue[26] to allow more accurate determination of the dielectric properties at the nanotube interior interface as a function of immersing solvent.

Observing Capillary Wetting. It is apparent from the results thus far that the OTS-modified nanotubes remain dry in water and are filled in pure methanol. An important implication of the Young−Laplace theory of capillarity is that the sign of the capillary pressure depends only on the contact angle formed between the meniscus and the capillary wall. Therefore, in a capillary, one expects to see a discreet transition from nonwetting to wetting when the contact angle drops below 90°, and this transition should be independent of capillary size. An important objective of the current work is to determine if these expectations from the Young−Laplace equation hold at the nanoscale. To achieve this end we conducted a systematic study of nanotubes immersed in mixtures over a range of methanol mol fractions. The results of these experiments are shown in Figure 5 where the nanotube wettability is plotted against methanol mol fraction (X_{MeOH}). Note that we have defined wettability as the fraction of experiments in which FRAP was observed. Each point in Figure 5 is calculated from at least 14 FRAP measurements. Wettability values of zero indicate that FRAP was never observed in any of the bleaching experiments. A sharp transition from nonwetting to wetting conditions is observed as predicted by the Young−Laplace equation, and there is no significant difference between the results for the two nanotube sizes. During our experiments we made infrequent observations of anomalous wetting observed in the 170 nm i.d. nanotubes at $0 < X_{MeOH} < 0.5$, and these observations led to the small, nonzero values of wettability reported at low methanol mol fractions in Figure 5. These anomalous observations result from a few nanotubes with defect, and this is discussed in detail in the Supporting Information.

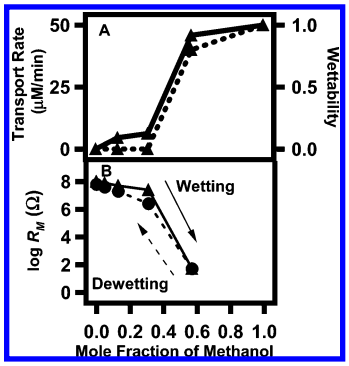

Figure 6. Results from measurements made with an OTS-modified nanotube membrane (i.d. = 170 nm). (A) Comparison of results from membrane transport studies (dotted line) with those from single nanotube wettability studies (solid line), i.d. = 170 nm. (B) Semilogarithmic plot of the membrane resistance, R_M, over a range of X_{MeOH}. R_M values were determined from ac impedance measurements and were conducted in electrolytic solutions of 0.1 M KCl. The value of R_M is diminished by ion flow when the membrane pores are wetted and is dramatically increased when the hydrophobic membrane pores are dry. The sharp decrease in the value of R_M above $X_{MeOH} = 0.31$ indicates that the membrane channels have filled. During the course of the experiment, methanol concentration was first increased and then decreased. Dewetting was observed as the mol fraction was decreased.

Membrane Transport Experiments. Our results from individual nanotube experiments, using FRAP and solvatochromism, provide a detailed view of the wetting behavior in individual nanotubes. These results should be extendable to describe the performance of membranes consisting of arrays of nanotubes. The template synthesis method is readily amenable to testing ensembles of nanotubes, since before final processing, the membrane itself is essentially an array of single nanotubes. Martin and co-workers have tested transport properties of nanotube membranes,[4,7] and we have employed similar techniques to investigate the transport of $DiIC_{18}$ across a membrane of 170 nm i.d. pores using the same methanol/water mixtures employed in our single-nanotube experiments. $DiIC_{18}$ was used in membrane transport experiments so that direct comparison with single-nanotube measurements would be valid. The transport experiments are used to measure the rate of $DiIC_{18}$ molecules diffusing across a membrane between a stock and receiver solution. Transport is monitored by UV−vis absorption of $DiIC_{18}$ in the receiver solution at the absorbance maxima given in Table 2. The molar extinction coefficients in Table 2 were used to calculate the concentrations by Beer's law. Figure 6A shows a comparison between transport measurements made with a nanotube membrane and our single-nanotube wettability studies. The transport rate mirrors the wettability. The good correlation between the two sets of experimental data strengthens our conclusion that nanotube wetting does not occur at methanol mol fractions of 0.3 or less.

It may be argued that strong partitioning of the permeant molecule to the hydrophobic nanotube interior could hinder or even facilitate transport. For instance, selective transport of toluene and pyridine through thiol-functionalized gold nanotube membranes has been demonstrated by the Martin group.[31] They proposed a mechanism whereby partitioning of hydrophobic molecules from the aqueous feed solution to the thiol layer facilitates transport across the membrane even though the pores

(31) (a) Hulteen, J. C.; Jirage, K. B.; Martin, C. R. *J. Am. Chem. Soc.* **1998**, *120*, 6603. (b) Jirage, K. B.; Hulteen, J. C.; Martin, C. R. *Anal. Chem.* **1999**, *71*, 4913.

remain unwetted by the water. This mechanism does not apply to our studies, since, relative to toluene and pyridine, $DiIC_{18}$ has a low vapor pressure, high molecular weight, and is a charged molecule. Additionally, the OTS layer on silica may not form a well-ordered monolayer as is seen for alkanethiols on gold.

ac Impedance Measurements. Measurements of ac impedance have been widely used to demonstrate ionic conductivity of membranes in aqueous solutions and offer a probe-free method for verifying the wetting behavior of our nanotubes membranes.[32] Nyquist analysis of impedance data reduces the apparent impedance to an equivalent circuit composed of solution resistance (R_S), membrane resistance (R_M), and membrane capacitance (C_M). From the best fit to the Nyquist plot the R_M and C_M values can be obtained. Here, the larger the membrane resistance, the smaller the ionic conductivity of the membrane. Membrane resistance values larger than 1 MΩ, in aqueous solution, imply that the membrane is dry inside since the ions (e.g., K^+ and Cl^-) cannot exist inside the nanotubes of the membrane due to their insolubility in the hydrophobic layers. Figure 6B shows a plot of membrane resistance versus mol fraction of methanol. Over the methanol mol fraction range of 0−0.31, very large values of R_M, >10 MΩ, were obtained, while the R_M value transitioned to ∼50 Ω at 0.57 methanol mol fraction. Interestingly, we found the wetting−dewetting process was reversible, with slight hysteresis. This is consistent with our previous results in which reversible wetting due to spontaneous cavitation was observed.[22,27]

Discussion

Nanotube samples with precise internal pore diameters and known surface chemistries provide a means to examine the behavior of fluids in well-defined nanoscale cylindrical containers, thus allowing us to solve problems relevant to nanofluidics and theoretical aspects of confined liquids. Our previous work focused on evaluating diffusion rates inside 200 nm i.d nanotubes under wetting conditions.[22,27] Here, we examine the wetting process itself, by investigating wettability as a function of both nanotube size and solvent composition and compare our results to prediction from the Young−Laplace equation.

In FRAP studies, we use the presence or absence of dye diffusion in hydrophobic nanotubes as a signature for wetting and nonwetting conditions, respectively. Transport and ac impedance studies conducted with intact nanotube membranes support our results from studies of individual nanotubes. As expected from conventional capillarity, both 30 and 170 nm i.d. nanotubes show a sharp transition from non-wetting to wetting as the mol fraction of methanol increases. The wetting transition, or nanotube filling, occurs near equimolar methanol/water concentrations for both nanotube diameters.

An approximate treatment of capillarity in macroscopic systems, such as glass capillary tubes, is traditionally made in terms of the Young−Laplace equation (eq 1). This approach assumes that the contact angle at the liquid/gas/solid interface (θ_c) will determine the concavity of the meniscus at the nanotube opening and that the meniscus is spherical with a radius of curvature equal to the capillary radius, r. The meniscus formed by a wetting solution ($\theta_c < 90°$) at the capillary opening will be concave with respect to the nanotube interior, and the capillary pressure will be positive. Alternatively, the meniscus formed by a nonwetting solution ($\theta_c > 90°$) will be convex with respect to the nanotube interior, and the capillary pressure will be negative.

The data in Figure 3 illustrate the limiting behaviors observed in FRAP experiments between nanotubes immersed in pure water versus nanotubes in pure methanol. In pure water, the absence of diffusion indicates that the nanotube interior is dry. This assignment is supported by the Young−Laplace equation and by observations from ordinary capillaries as illustrated in the Results. Therefore, it is not unexpected that the OTS-treated interior of nanotubes would remain dry in pure water regardless of the nanotube diameter. Figure 5 summarizes observations made over a range of methanol mol fractions (X_{MeOH}) and reveals the transition between wet and dry nanotubes.

An obvious question is the following: does the Young−Laplace equation describe the wettability of our nanotubes? The capillary pressures given in Table 1 were calculated using contact angles measured for water on OTS-modified glass. Since a positive capillary pressure promotes filling, nanotube filling should occur at $X_{MeOH} > 0.05$. The results from our wettability studies summarized in Figure 5 show that a clear transition from nonwetting to wetting conditions exists close to $X_{MeOH} = 0.5$, a value approximately 10 times greater than that predicted by the Young−Laplace equation. A possible explanation for the observed discrepancy between our experimental results and the theoretical predictions of Table 1 may be that the samples have simply not equilibrated by the time the measurements are made. To ensure that our results reflect equilibrium conditions, we conducted experiments on a single sample over a period of 2 days. Figure 5B shows the results for samples which were allowed to equilibrate for at least 24 h. Very little difference is measured between the 2 days. The entrapment of air inside the nanotubes as they are immersed could provide a possible explanation for the unusual wettability results. However, this argument can be countered since it is unlikely that trapped air would remain in the nanotubes for 24 h given the gas permeability of the nanotube walls and the immense capillary pressures in Table 1.

The failure of the Young−Laplace equation to predict the wetting behavior of hydrophobic nanotubes is interesting and should be addressed since it obviously impacts a range of potential applications involving nanoscale fluid-based devices. A recent study by Helmy et al. have shown that the Young−Laplace underestimates capillary pressure by as much as a factor of 2 for water in hydrophobic pores of a few nanometers.[16] Here we have complemented these studies by directly observing the change in capillary pressure that occurs with the addition of a cosolvent.

Theoretical treatments of confined fluids[19,21,22] may provide explanations for the failure of conventional capillarity at the nanoscale. These explanations stem from issues of phase stability in confined liquids. Critical diameters for the phase stability of liquid water in slitlike pores has been estimated at ∼100 nm.[19] In cylindrical pores the critical diameter will be even greater and has been calculated to be as much as several micrometers.[21] Phase instability occurs when the chemical potentials of the vapor and liquid phase are equal. Spontaneous fluctuations of

(32) (a) Ikematsu, M.; Iseki, M.; Sugiyama, Y.; Mizukami, A. *Biosystems* **1995**, *35*, 123. (b) Steinle, E. D.; Mitchell, D. T.; Wirtz, M.; Lee, S. B.; Young, V. Y.; Martin, C. R. *Anal. Chem.* **2002**, *74*, 2416. (c) Ding, L.; Li, J. H.; Dong, S. J.; Wang, E. K. *J. Electroanal. Chem.* **1996**, *416*, 105.

vapor layers formed near the hydrophobic surface and the surface tension of the solvent can lead to spontaneous cavitation even in a filled volume. In our case, the liquid phase never fills the volume until a much higher methanol mol fraction than that predicted by the Young−Laplace equation is reached. Instability of the liquid phase in the hydrophobic pore may be responsible for the anomalous capillarity. It is also possible that the discrepancy could arise from our dependence on macroscopic contact angles acquired from flat surfaces or from changes in the liquids surface tension when the meniscus is highly curved. Sobolev et al. have addressed this issue and shown that surface tension of water in quartz capillaries with radii down to 40 nm is unchanged from that of bulk but find a steep dependence of the observed contact angle on meniscus velocity.[33] Until contact angles and menisci shape at the nanoscale can be directly measured or accurately calculated, predictions of wettability in nanotubes will rely on parameters gleaned from macroscopic observations or on direct measurements as presented here. We have shown that direct measurement is more reliable.

Conclusions

We have used an improved SSG template synthesis to prepare silica nanotubes within the pores of alumina template membranes with the means to control the wall thickness. Using this method we produced nanotubes with both 30 and 170 nm i.d. Both sizes were prepared with hydrophobic interior surfaces achieved through covalent attachment of OTS. Wettability of the nanotube interior was investigated using FRAP, solvatochromism, membrane transport, and ac impedance measurements. Results from these experiments provide a quantity of evidence indicating that simple capillarity considerations fail to provide an adequate prediction of the wetting behavior in hydrophobic nanotubes of both 30 and 170 nm i.d. A sharp transition that is independent of nanotube size is observed between wetting and nonwetting conditions as expected. However, the transition occurs at a much higher methanol mol fraction than that predicted by the Young−Laplace equation. The origin of this discrepancy remains unclear but may be due to our reliance on macroscopic values of contact angles, or it may be related to liquid-phase instability within the hydrophobic pore. The reversibility of the wetting transition suggests that phase instability may be the primary source of the anomalous wetting behavior.

Our results are critically important for the successful implementation of nanotubes as nanofluidic devices, in separations, and for biomedical applications such as drug delivery, or as miniature reaction vessels. Understanding solvent wetting properties in nanotubes and how these properties vary from macroscopic models will provide a framework for the design of nanotubes with surface chemistries tailor-made for specific applications. The use of single-nanotube measurements provides a detailed view of solvent−nanotube interactions that is unachievable with bulk measurements. Our single-nanotube approach, illustrated here with hydrophobic nanotubes, is a promising new method and is adaptable to investigations using silica nanotubes with a wide range of surface chemistries.

Acknowledgment. This work was supported in part by the National Science Foundation MRSEC-DMR No. 0080008 and by UMD start-up funds to both S.B.L. and D.S.E.

Supporting Information Available: Additional observations. This material is available free of charge via the Internet at http://pubs.acs.org.

JA055535C

(33) Sobolev, V. D.; Churaev, N. V.; Velarde, M. G.; Zorin, Z. M. *J. Colloid Interface Sci.* **2000**, *222*, 51.